

1 **Identification of SARS-CoV2 Main Protease Coldspots Suitable for Drug Targeting**

2

3 Navaneethakrishnan Krishnamoorthy^{1,*} and Khalid Fakhro^{1,2,3}

4

5 ¹Department of Human Genetics, Sidra Medicine, Doha, Qatar

6 ²Department of Genetic Medicine, Weill Cornell Medical College, Doha, Qatar

7 ³College of Health and Life Sciences, Hamad Bin Khalifa University, Doha, Qatar

8 *Correspondence: nkrishnamoorthy2@sidra.org

9

10 Most attempts to target the novel coronavirus SARS-CoV2 are focusing on the main protease
11 (M^{pro})¹⁻⁹. However, >19,000 missense mutations in the M^{pro} have already been reported¹⁰. The
12 mutations encompassing 282 amino acid positions and these “hotspots” might change the M^{pro}
13 structure and activity, potentially rendering novel antivirals and vaccines ineffective. Here we
14 identified 24 mutational “coldspots” that have resisted mutation since the virus was first
15 detected. We compared the structure-function relationship of these coldspots with several
16 SARS-CoV2 M^{pro} X-ray crystal structures. We found that three coldspot residues (Leu141,
17 Phe185 and Gln192) help to form the active site, while six (Gly2, Arg4, Tyr126, Lys137,
18 Leu141 and Leu286) contribute to dimer formation that is required for M^{pro} activity. The
19 surface of the dimer interface is more resistant to mutations compared to the active site.
20 Interestingly, 16 coldspots are found in conserved patterns when compared with other
21 coronaviruses. Importantly, several conserved coldpots are available on the surface of the
22 active site and at the dimer interface for targeting. The identification and short list of these
23 coldspots offers a new perspective to target the SARS-CoV2 M^{pro} while avoiding mutation-
24 based drug resistance.

25 Keywords: Mutation Hotspot, X-ray Structure, Missense Mutation, Structure-function
26 Relationship, Dimer interface, Mutation-based Drug Resistance

27

28 *Mutational hotspots and coldspots*

29

30 The SARS-CoV2 main protease (M^{pro}) or 3CL-protease (3CL pro) is essential for its proteolytic
31 activity, structural protein production and host cell infection¹¹. Early in the COVID-19
32 pandemic, mutational hotspots were reported within SARS-CoV2 genomic sequences^{12,13}.
33 Mutational coldspots within viral genomes and/or proteins can indicate the location of
34 appropriate targets for therapeutics that can evade mutation-based drug-resistance. However,

35 mutational coldspots with no known mutations have not been examined in the amino acid
36 sequence and 3D structure of SARS-CoV2 M^{pro}. To identify these coldspots in SARS-CoV2
37 M^{pro}, we aggregated the circulating missense mutations reported in Global Initiative on Sharing
38 All Influenza Data (GISAID) until November 2, 2020. This was approximately 11 months since
39 the start of the COVID-19 outbreak, which should have provided enough time for the virus to
40 accumulate some key mutations for survival ^{13,14}. The dataset contained 19,154 mutations (see
41 supplementary Table S1 for the details) covering total of 282 out of 306 residue positions of
42 SARS-CoV2 M^{pro} which are referred here as mutational hotspots (Fig. 1a and 1b). These
43 hotspots showed a minimum of one mutation (Fig. 1a). In particular, the data (top 13 with >200
44 mutations) showed the following hotspot positions were the most frequently mutated: Gly15
45 (6,297 reported mutations), Leu89 (2,392), Gly71 (1,615), Lys90 (1,108), and Asp248 (744)
46 (Fig. 1b). The remaining 24 positions had no reported mutations and were considered
47 mutational coldspots (Fig. 1c), as they have shown a degree of mutation resistance up to this
48 stage of the pandemic. Although the 24 mutational coldspots are shortlisted from 306 residues,
49 we studied structures of SARS-CoV2 M^{pro} to understand their structure-functional relevance.

50

51 *Coldspots at the active/inhibitor site*

52 To analyze the coldspots in and around the active site, we selected five 3D-structures with high
53 resolution (Protein Data Bank (PDB) codes: 6LU7, 6Y2F, 6LZE, 6M0K, and 7BUY), out of
54 several SARS-CoV2 M^{pro} structures, that had been co-crystallized with antiviral drug
55 candidates in recently published studies ^{3,5,6,9}. However, the inhibitors were not optimal for
56 SARS-CoV2 ¹⁵. We believe the non-mutational residues (coldspots) could be appropriate target
57 regions for designing effective inhibitors of SARS-CoV2 M^{pro}. In the SARS-CoV2 M^{pro}
58 structures, domains I (8-101) and II (102-185) play major roles in the formation of the active

59 site and provide binding sites for inhibitors; while domain III (202-306) is important in the
60 regulation of protease activity^{3,9}. The catalytic dyad His41 and Cys145 is located at the active
61 site that forms in a cleft between domain I and II. Most efforts to design anti-viral inhibitors
62 using drug repurposing approaches are focused on targeting this active site^{3,11}. We found 15
63 coldspots to be from domains I and II, and the remaining nine were in domain III (Fig. 1c). The
64 inhibitor-binding sites in the five SARS-CoV2 M^{pro} structures were superimposed and are
65 represented as a surface model in the 3D structures (Fig. 1d, 1e and 1f), which show that a total
66 of 25 residues (Fig. 1g) form the binding sites for the reported inhibitors (6LU7-N3 (M^{pro}-
67 inhibitor name), 6Y2F-13b, 6LZE-11a, 6M0K-11b, and 7BUY-carmofur). In these 25
68 positions, 22 were affected by a total of 525 mutations. In particular, residue positions 46, 49,
69 142, 190, and 191 showed more than 15 mutations each. This result suggests that most of the
70 active site residues are mutated and challenging to target.

71

72 Interestingly, we mapped three coldspots, Leu141, Phe185, and Gln192, in the 6LU7-N3
73 complex (Fig. 1f). The structural importance of these coldspots was emphasized by the recent
74 X-ray crystallographic studies of SARS-CoV2 M^{pro}^{4,5,7} demonstrating the involvement of the
75 spots in the formation of substrate-binding sites and Phe185 and Gln192 in the stability of the
76 active site. We found coldspots Asn133 and Lys137 beneath the surface formed by the binding-
77 site residues (Fig. 1e), specifically, Leu27, Asn119, and Gly146 are near the catalytic dyad
78 (His41 and Cys145). They may provide some support to the catalytic center, as evidenced by
79 a recent study, in which Leu27 was found to play a key role in the activity of the M^{pro} structure
80 of SARS-CoV2⁸. Whereas, Leu27 and Asn119 are involved in the formation of the binding
81 site in SARS-CoV M^{pro}¹⁶ (Table 1). However, based on our data analysis, the other pocket-
82 forming residues in the structures undergo mutations, which may modify the shape of the
83 binding pocket. This prediction is supported by a recent study¹⁷, in which the structures of the

84 mutants Met49Ile, Pro184Leu/Ser, and Ala191Val were shown to substantially deviate from
85 the wildtype. Thus, the residues were assumed to belong within the mobile regions of the active
86 site, which control the conformational changes that may be required for catalysis. This indicates
87 that coldspots are required at the active site to maintain effective targeting.

88 Most importantly, in SARS-CoV2 M^{pro}, the key active site residues His41 (3 mutations),
89 Phe140 (1 mutation), Cys145 (3 mutations), Glu166 (3 mutations), and His172 (1 mutation)
90 showed low mutation frequencies (a total of eleven out of 525 mutations at the active site) (Fig.
91 1g). This suggests that the residues involved in critical functions at the active site are mutated
92 less frequently than other residues.

93

94 *Coldspots at the dimer interface*

95 An alternate therapeutic strategy is to design antiviral agents to target the dimerization of the
96 SARS-CoV M^{pro}, as the dimeric form is essential for activity ^{18,19} and, with 98% identity, is
97 also applicable to SARS-CoV2 M^{pro} ^{4,7}. Here, we examined the functional relevance of
98 coldspots on the surface of the dimer interface in SARS-CoV2 (PDB code: 6LU7), as they
99 could provide mutation-resistant drug and vaccine target sites (Fig. 2a). Half of the 24 coldspot
100 positions are on the surface of the protease (Fig. 2a-2b), and the rest are buried. We discovered
101 seven cold spot positions (Gly2, Arg4, Tyr126, Lys137, Leu141, Leu286, and Leu287) on the
102 surface that are involved in the formation of the dimer interface in the SARS-CoV2 M^{pro} (Fig.
103 2c and 2d). They form two sites: the first is based on the positions Gly2, Arg4, Tyr126, Lys137,
104 and Leu141 (Fig. 2c), and the second site includes the positions Arg4, Lys137, Leu286, and
105 Leu287 (Fig. 2d). In the SARS-CoV M^{pro}, these sites include several key interactions, Arg4-
106 Lys137-Glu290 ²⁰, Gly2-Arg4-Tyr126 ²¹, Ser284-Tyr285-L286 ²², and Ser1-Glu166-His163-

107 His172^{23,24}, that have been experimentally proven to be vital for maintaining the dimer
108 interface and the active site (Table 1).

109

110 In SARS-CoV2 M^{pro}, we observed a hydrogen bond between Arg4 and Lys137 (Fig.2c). As
111 both are coldspots (with three other coldspots nearby, Gly2, Tyr126, and Leu141), this appears
112 to be a potential site for inhibition. It also appears slightly similar to the one recently proposed
113 as a potential allosteric site in SARS-CoV2 M^{pro}⁴. Residue 141 plays a dual role by forming
114 the active site and dimer interface with Val303 (Fig.1e, 1f and 2c). Leu286 forms two hydrogen
115 bonds with Ser284 in protomer A and hydrophobic interactions with Tyr280, Gly283, and
116 Ala285 in protomer B. Moreover, eight other coldspot residues (Asn119, Asn133, Tyr154,
117 Phe185, Gln192, Gln256, Gly258, and Asp295) on the protease surface (Fig. 2a and 2b) and
118 do not contribute to the dimer interface.

119

120 The other structures of SARS-CoV2 M^{pro} also confirms the functional relevance of the coldspot
121 residues Gly2, Arg4, Tyr126, Lys137, Leu141, and Leu286 that are directly involved in dimer
122 formation through various interactions^{7,9} (Table 1). A recent electrophilic screening of 1,250
123 fragments provided three hits (Z1849009686, Z264347221, and POB0073) that bind to the
124 dimer interface, and it was suggested these fragments might be used as quasi-allosteric
125 inhibitors to disrupt the dimerization of the active M^{pro}⁴. The coldspots Gly2 and Leu141 are
126 involved in the reported binding sites for fragment Z264347221, while Arg4 and Lys137 are
127 involved in POB0073 binding. Furthermore, Glu286 is conserved at the interface of M^{pro} in
128 Porcine epidemic diarrhea virus (PEDV), Transmissible gastroenteritis virus, Infectious
129 bronchitis virus (TGEV), and Human coronavirus 229E (HCOV-229E)²⁵⁻²⁷. We noted that
130 Leu286 makes vital hydrophobic contacts at the dimer interface in SARS-CoV2 M^{pro}. Tyr126

131 is another critical residue for dimer formation of M^{pro} in SARS-CoV, PEDV ²⁷, TGEV ²⁵, and
132 HCoV-229E ²⁶ and, together with 141, is involved in the regulation of catalytic activity ^{21,28}.
133 These correlate with our hypothesis that the observed coldspots may serve as mutation-resistant
134 allosteric sites.

135

136 There are 21 hotspots at the interface covering 296 mutations; out of 21, only 10 hotspots had
137 more than eight mutations (Fig. 2e). The frequency of mutations was very high at residue
138 positions Gly283, Ala285, and Arg298 (65, 51, and 52 mutations, respectively), compared with
139 the hotspots at the N-finger (residue 1-8) region. Mutational frequency (296) of surface
140 residues at the dimer interface is relatively less than the active site residues (525 mutations)
141 (Fig.1g). This indicates that the dimer interface at SARS-CoV M^{pro} seems to be more resistant
142 to mutations.

143

144 *Coldspots conserved among coronaviruses*

145 Furthering our understanding of those residues conserved among coronaviruses (CoVs) might
146 provide optimum target regions for designing improved therapeutic agents ²⁹. We compared
147 the coldspots of SARS-CoV2 with other CoVs to analyze their degree of conservation. The
148 structure-based sequence alignment of 12 different CoVs shows that the majority of the
149 coldspots are arranged as three clusters: four coldspots at the N-terminal, six near the C-
150 terminal and, surprisingly, nine near the active site in domain II (Fig. 3). We found 16 coldspots
151 are distributed in eight conserved blocks including a block GxcGSvGxn based on motif
152 GSCGS that is essential for the initiation of the catalysis in MERS-CoV and SARS-CoV ^{15,30}.
153 Similarly, the other conserved blocks might have some functional role as they are found in the
154 key structural regions. Interestingly, 14 out of the 24 coldspots were conserved among all the

155 CoVs. Moreover, most of the 14 conserved coldspots of SARS-CoV2 M^{pro} have critical roles
156 in the formation of the active site (Leu27 and Gln192) and at the dimer interface (Gly2, Cys16,
157 Lys137, Leu287, and Asp295), and Leu141 has both roles (Table 1, Fig. 2 & Fig. 3). The
158 significance of the other conserved coldspots (Asn133, Gly146, Asn203, Phe219, Asn231, and
159 Gly258) in SARS-CoV2 M^{pro} are unclear. Overall, this sequence alignment suggests that not
160 all the highly conserved residues in SARS-CoV2 M^{pro} are resistant to mutation. Although only
161 certain coldspots are conserved among CoVs, most of the conserved sites contribute to the
162 formation of critical interactions (Table 1).

163

164 *Biological relevance*

165 It is understood that the SARS-CoV2 M^{pro} is undergoing or accumulating mutations at many
166 hotspots, thus it is essential to identify consistent mutational coldspots that can be targeted with
167 antiviral drugs. In addition, the data of nearly 20,000 global mutations used in this study were
168 collected at the end of the first wave of COVID-19, are minimal. However, the identified
169 mutational coldspots have biological relevance, according to the high-resolution X-ray
170 structures of SARS-CoV2, sequence conservation among CoVs, and experimental evidence
171 provided by the published X-ray structures of other CoV proteases^{18,22,23,25-28,31,32} (Table 1).
172 We now have a short list of promising targets that might be considered before embarking on
173 time-consuming translational research underlying antiviral design.

174

175 The observed mutational frequencies in the hotspots at the active site and dimer interface
176 indicate that the virus may be developing protective strategies against inhibitors. This correlates
177 with the findings described in recent reports, which show the positions are changing the shape
178 of the sites via mutations and plasticity^{17,33}. However, coldspots that are identified here might

179 be good areas to target. Although some of these coldspots may convert to hotspots in the future,
180 the frequency of the new mutations is likely to be minimal, as the data in this study show the
181 sites play critical structural roles and are mutation-resistant. This is evident from their ability
182 to avoid mutations over 11 months since the virus was first detected. However, further research
183 is warranted for a deeper understanding of the phenomenon.

184

185 In conclusion, mutations in SARS-CoV2 M^{pro} delay the structure-based design of antivirals.
186 This study highlighted the existence of various mutation-resistant coldspots and investigated
187 their significance using evidence from structural studies. We have conducted initial filtering of
188 the mutations of structural importance and reduced the data from 306 residues to 24 mutation
189 coldspots. Finally, we pinpointed several conserved coldspots at the surface of the active site
190 and dimer interface that could be optimum targets for the design of mutation-resistance
191 antivirals.

192

193

194 Methods

195 Mutation dataset

196 The missense mutation dataset consisting of the reported circulating non-synonymous
197 replacement mutations of SARS-CoV2 M^{pro} was retrieved from GISAID¹⁰ by searching
198 (CoVsurre) the database against the reference protein sequence Wuhan-Hu-1 (NC_045512.2,
199 10,055-10,977) with 306 amino acid positions. The dataset was collected until November 2,
200 2020. There were 19,154 mutations (see supplementary Table S1 for the details) at 282 residue
201 positions, which were considered as mutational hotspots. The data were consolidated based on

202 the residue positions to calculate their mutational frequencies. This led to the discovery of 24
203 positions with no reported mutations at the time of collection, which were considered SARS-
204 CoV2 M^{pro} mutational coldspots. The 24 coldspots were used for structural and sequence
205 analyses.

206

207 Structural analyses

208 Recently published high-resolution dimeric (protomer A and B) X-ray 3D structures of SARS-
209 CoV2 M^{pro} were obtained from the PDB (codes: 6LU7, 6Y2F, 6LZE, 6M0K, and 7BUY)^{3,5,6,9},
210 and the M^{pro} structures of other CoVs determined in previous studies were used for structural
211 investigations. The 3D-locations of the hotspot and coldspot residues within key functional
212 regions were mapped in the structures of SARS-CoV2 M^{pro}. To examine the substrate-binding
213 sites, we used the structures of SARS-CoV2 M^{pro} and inhibitor co-crystals (6LU7-N3, 6Y2F-
214 13b, 6LZE-11a, 6M0K-11b, and 7BUY-carmofur) and generated a pocket surface model with
215 all pocket-forming residues. Pymol was used for structural analyses and to represent the
216 molecular structures (The PyMOL Molecular Graphics System, Schrödinger, LLC.).

217

218 Sequence alignment

219 In the structure-based sequence alignment, to represent the coronavirus superfamily³⁴, we used
220 11 structural-sequences of M^{pro} from different families. The following M^{pro} sequences of CoVs
221 with X-ray structures (PDB codes: 2HOB Severe acute respiratory syndrome coronavirus
222 (SARS-CoV), 4YOI Tylonycteris bat coronavirus HKU4 (HKU4), 4ZUH Porcine epidemic
223 diarrhea virus (PEDV), 2ZU2 Human coronavirus 229E (HCOV-229E), 4WME Middle East
224 respiratory syndrome-related coronavirus (MERS), 6JIJ Murine hepatitis virus strain A59
225 (MURINE), 3D23 Human coronavirus HKU1 (isolate N1) (HKU1-N1), 6FV2 Human

226 coronavirus NL63 (HCOV-NL63), 4ZRO Feline infectious peritonitis virus (strain 79-1146)
227 (FIPV), 2AMP Transmissible gastroenteritis virus, Infectious bronchitis virus (TGEV), 2Q6F
228 Infectious bronchitis virus (IBV)) were used in a multiple sequence alignment against M^{PRO} of
229 SARS-CoV2 (6LU7) as a reference. We used Multalign for the multiple sequence alignment³⁵.

230

231

232 References

- 233 1 Liu, C. *et al.* Research and Development on Therapeutic Agents and Vaccines for
234 COVID-19 and Related Human Coronavirus Diseases. *ACS Central Science*,
235 doi:10.1021/acscentsci.0c00272 (2020).
- 236 2 Luan, B., Huynh, T., Cheng, X., Lan, G. & Wang, H. R. Targeting Proteases for
237 Treating COVID-19. *J Proteome Res* **19**, 4316-4326,
238 doi:10.1021/acs.jproteome.0c00430 (2020).
- 239 3 Dai, W. *et al.* Structure-based design of antiviral drug candidates targeting the SARS-
240 CoV-2 main protease. *Science (New York, N.Y.)* **368**, 1331-1335,
241 doi:10.1126/science.abb4489 (2020).
- 242 4 Douangamath, A. *et al.* Crystallographic and electrophilic fragment screening of the
243 SARS-CoV-2 main protease. *Nature communications* **11**, 5047, doi:10.1038/s41467-
244 020-18709-w (2020).
- 245 5 Jin, Z. *et al.* Structure of M(pro) from SARS-CoV-2 and discovery of its inhibitors.
246 *Nature* **582**, 289-293, doi:10.1038/s41586-020-2223-y (2020).
- 247 6 Jin, Z. *et al.* Structural basis for the inhibition of SARS-CoV-2 main protease by
248 antineoplastic drug carmofur. *Nat Struct Mol Biol* **27**, 529-532, doi:10.1038/s41594-
249 020-0440-6 (2020).
- 250 7 Kneller, D. W. *et al.* Unusual zwitterionic catalytic site of SARS-CoV-2 main protease
251 revealed by neutron crystallography. *The Journal of biological chemistry*,
252 doi:10.1074/jbc.AC120.016154 (2020).
- 253 8 Rut, W. *et al.* SARS-CoV-2 M(pro) inhibitors and activity-based probes for patient-
254 sample imaging. *Nature chemical biology*, doi:10.1038/s41589-020-00689-z (2020).
- 255 9 Zhang, L. *et al.* Crystal structure of SARS-CoV-2 main protease provides a basis for
256 design of improved alpha-ketoamide inhibitors. *Science (New York, N.Y.)* **368**, 409-
257 412, doi:10.1126/science.abb3405 (2020).
- 258 10 Shu, Y. & McCauley, J. GISAID: Global initiative on sharing all influenza data - from
259 vision to reality. *Euro Surveill* **22**, doi:10.2807/1560-7917.ES.2017.22.13.30494
260 (2017).
- 261 11 Ullrich, S. & Nitsche, C. The SARS-CoV-2 main protease as drug target. *Bioorganic*
262 & *medicinal chemistry letters* **30**, 127377, doi:10.1016/j.bmcl.2020.127377 (2020).
- 263 12 Pachetti, M. *et al.* Emerging SARS-CoV-2 mutation hot spots include a novel RNA-
264 dependent-RNA polymerase variant. *Journal of translational medicine* **18**, 179,
265 doi:10.1186/s12967-020-02344-6 (2020).
- 266 13 Badua, C., Baldo, K. A. T. & Medina, P. M. B. Genomic and proteomic mutation
267 landscapes of SARS-CoV-2. *Journal of medical virology*, doi:10.1002/jmv.26548
268 (2020).
- 269 14 Korber, B. *et al.* Tracking Changes in SARS-CoV-2 Spike: Evidence that D614G
270 Increases Infectivity of the COVID-19 Virus. *Cell* **182**, 812-827 e819,
271 doi:10.1016/j.cell.2020.06.043 (2020).
- 272 15 Ionescu, M. I. An Overview of the Crystallized Structures of the SARS-CoV-2. *Protein*
273 *J*, doi:10.1007/s10930-020-09933-w (2020).
- 274 16 Xue, X. *et al.* Structures of two coronavirus main proteases: implications for substrate
275 binding and antiviral drug design. *Journal of virology* **82**, 2515-2527,
276 doi:10.1128/JVI.02114-07 (2008).
- 277 17 Sheik Amamuddy, O., Verkhivker, G. M. & Tastan Bishop, O. Impact of Early
278 Pandemic Stage Mutations on Molecular Dynamics of SARS-CoV-2 M(pro). *Journal*

- 279 *of chemical information and modeling* **60**, 5080-5102, doi:10.1021/acs.jcim.0c00634
280 (2020).
- 281 18 Hsu, W. C. *et al.* Critical assessment of important regions in the subunit association and
282 catalytic action of the severe acute respiratory syndrome coronavirus main protease.
283 *The Journal of biological chemistry* **280**, 22741-22748, doi:10.1074/jbc.M502556200
284 (2005).
- 285 19 Goyal, B. & Goyal, D. Targeting the Dimerization of the Main Protease of
286 Coronaviruses: A Potential Broad-Spectrum Therapeutic Strategy. *ACS combinatorial*
287 *science* **22**, 297-305, doi:10.1021/acscombsci.0c00058 (2020).
- 288 20 Ghosh, A. K. *et al.* Design and synthesis of peptidomimetic severe acute respiratory
289 syndrome chymotrypsin-like protease inhibitors. *Journal of medicinal chemistry* **48**,
290 6767-6771, doi:10.1021/jm050548m (2005).
- 291 21 Wei, P. *et al.* The N-terminal octapeptide acts as a dimerization inhibitor of SARS
292 coronavirus 3C-like proteinase. *Biochemical and biophysical research communications*
293 **339**, 865-872, doi:10.1016/j.bbrc.2005.11.102 (2006).
- 294 22 Lim, L., Shi, J., Mu, Y. & Song, J. Dynamically-driven enhancement of the catalytic
295 machinery of the SARS 3C-like protease by the S284-T285-I286/A mutations on the
296 extra domain. *PloS one* **9**, e101941, doi:10.1371/journal.pone.0101941 (2014).
- 297 23 Xue, X. *et al.* Production of authentic SARS-CoV M(pro) with enhanced activity:
298 application as a novel tag-cleavage endopeptidase for protein overproduction. *Journal*
299 *of molecular biology* **366**, 965-975, doi:10.1016/j.jmb.2006.11.073 (2007).
- 300 24 Tan, J. *et al.* pH-dependent conformational flexibility of the SARS-CoV main
301 proteinase (M(pro)) dimer: molecular dynamics simulations and multiple X-ray
302 structure analyses. *Journal of molecular biology* **354**, 25-40,
303 doi:10.1016/j.jmb.2005.09.012 (2005).
- 304 25 Anand, K. *et al.* Structure of coronavirus main proteinase reveals combination of a
305 chymotrypsin fold with an extra alpha-helical domain. *The EMBO journal* **21**, 3213-
306 3224, doi:10.1093/emboj/cdf327 (2002).
- 307 26 Lee, C. C. *et al.* Structural basis of inhibition specificities of 3C and 3C-like proteases
308 by zinc-coordinating and peptidomimetic compounds. *The Journal of biological*
309 *chemistry* **284**, 7646-7655, doi:10.1074/jbc.M807947200 (2009).
- 310 27 Ye, G. *et al.* Structural basis for the dimerization and substrate recognition specificity
311 of porcine epidemic diarrhea virus 3C-like protease. *Virology* **494**, 225-235,
312 doi:10.1016/j.virol.2016.04.018 (2016).
- 313 28 Shi, J., Sivaraman, J. & Song, J. Mechanism for controlling the dimer-monomer switch
314 and coupling dimerization to catalysis of the severe acute respiratory syndrome
315 coronavirus 3C-like protease. *Journal of virology* **82**, 4620-4629,
316 doi:10.1128/jvi.02680-07 (2008).
- 317 29 Naqvi, A. A. T. *et al.* Insights into SARS-CoV-2 genome, structure, evolution,
318 pathogenesis and therapies: Structural genomics approach. *Biochimica et biophysica*
319 *acta. Molecular basis of disease* **1866**, 165878, doi:10.1016/j.bbadis.2020.165878
320 (2020).
- 321 30 Wang, H. *et al.* Comprehensive Insights into the Catalytic Mechanism of Middle East
322 Respiratory Syndrome 3C-Like Protease and Severe Acute Respiratory Syndrome 3C-
323 Like Protease. *ACS Catal* **10**, 5871-5890, doi:10.1021/acscatal.0c00110 (2020).
- 324 31 Chen, S. *et al.* Residues on the dimer interface of SARS coronavirus 3C-like protease:
325 dimer stability characterization and enzyme catalytic activity analysis. *Journal of*
326 *biochemistry* **143**, 525-536, doi:10.1093/jb/mvm246 (2008).
- 327 32 Tomar, S. *et al.* Ligand-induced Dimerization of Middle East Respiratory Syndrome
328 (MERS) Coronavirus nsp5 Protease (3CLpro): IMPLICATIONS FOR nsp5

329 REGULATION AND THE DEVELOPMENT OF ANTIVIRALS. *The Journal of*
330 *biological chemistry* **290**, 19403-19422, doi:10.1074/jbc.M115.651463 (2015).
331 33 Kneller, D. W. *et al.* Structural plasticity of SARS-CoV-2 3CL M(pro) active site cavity
332 revealed by room temperature X-ray crystallography. *Nature communications* **11**, 3202,
333 doi:10.1038/s41467-020-16954-7 (2020).
334 34 Chen, Y., Liu, Q. & Guo, D. Emerging coronaviruses: Genome structure, replication,
335 and pathogenesis. *Journal of medical virology* **92**, 418-423, doi:10.1002/jmv.25681
336 (2020).
337 35 Corpet, F. Multiple sequence alignment with hierarchical clustering. *Nucleic Acids Res*
338 **16**, 10881-10890, doi:10.1093/nar/16.22.10881 (1988).
339 36 Rathnayake, A. D. *et al.* 3C-like protease inhibitors block coronavirus replication in
340 vitro and improve survival in MERS-CoV-infected mice. *Science translational*
341 *medicine* **12**, doi:10.1126/scitranslmed.abc5332 (2020).
342 37 Shi, J. & Song, J. The catalysis of the SARS 3C-like protease is under extensive
343 regulation by its extra domain. *The FEBS journal* **273**, 1035-1045, doi:10.1111/j.1742-
344 4658.2006.05130.x (2006).

345

346 Acknowledgement

347 We acknowledge GISAID for disseminating SARS-CoV2 data. We would like to thank all the
348 communities worldwide involved and supported in the response to the COVID- 19 pandemic.

349

350 Competing interests

351 The authors declare no competing interests.

352

353 Table

354 Table 1. Structural and functional importance of mutational coldspots in SARS-CoV2

S. no	Coldspot residue position	Structural and/or functional role	Publication	Experimental method
1	2, 4, 137	Gly2, Arg4 and Lys137 in the binding pocket at the dimer interface of SARS-CoV2 M ^{pro} for the inhibitor POB0073.	Douangamath et al., ⁴	Crystallographic and electrophilic fragment screening
	141	141 is involved in the formation of the binding site at the dimer interface of SARS-CoV2 M ^{pro} for the fragment/inhibitor Z264347221		
2	16	Cys16 Forms hydrogen bonds with Ser10, Gly11, and Glu14 in SARS-CoV2 M ^{pro} at the dimer interface	Kneller et al., ⁷	Neutron X-ray crystallography
3	27	Leu27 is involved in the activity of SARS-CoV2 M ^{pro} . It interacts with active binding probe, Biotin-PEG(4)-Abu-Tle-Leu-Gln-VS (B-QS1-VS)	Rut et al., ⁸	Synthesis and X-ray crystallography
4	192, 185, 141, 2, 4, 126, 137, 141, 286	Leu141, Phe185, Gln192 are involved in formation of inhibitor N3-binding pocket, and Gly2, Arg4, Tyr126, Lys137, Leu141, Leu286, and Leu287 function in the dimerization of SARS-CoV2 M ^{pro}	Jin et al., ⁵	X-ray crystallography
5	286	In SARS-CoV2 M ^{pro} , Ala285 and Leu286 induced slightly closer packing at the dimer interface and increased catalytic activity (compared to SARS-CoV M ^{pro})	Zhang et al., ⁹	X-ray crystallography
6	192	In MERS-CoV infected mice, residue 192 in M ^{pro} interacts with compound 6h and has a potential specificity role in selection of inhibitors 7j and 7i	Rathnayake et al., ³⁶	Therapeutic treatment in a mouse model, X-ray crystallography
7	185, 192	In SARS-CoV2 M ^{pro} , a long loop Phe185-194 is stabilized by the interactions of 189-192-186. Phe185 and Leu167 form a deep hydrophobic pocket for substrate binding	Kneller et al., ⁷	Neutron X-ray crystallography
8	2, 4, 16, 119, 137, 141	In SARS-CoV2 M ^{pro} at the dimer interface, N-terminal residues 1-16 (N-finger) interact with 118 (in protomer B)-125 (B) and loop 137 (B) -142 (B)	Kneller et al., ⁷	Neutron X-ray crystallography
9	4, 27, 141, 185, 295	Glu185 (in PEDV M ^{pro}) and Val185 (in SARS-CoV M ^{pro}) located in motif 3 of the substrate binding pocket. In PEDV M ^{pro} , Leu27 and Asn141 are two key residues involved in enzyme catalytic activity. Arg4Ala and Gln295Ala mutations at the dimer interface reduced the catalytic activity	Ye et al., ²⁷	X-ray crystallography, size-exclusion chromatography, and ultra-centrifugation
10	128, 137, 185,	In MERS CoV M ^{pro} , Lys137 and Glu290 form hydrophobic contacts with 185, and 128 forms van der Waals interactions with His8-Lys155. These residues are involved in control of the dimer interface	Tomar et al., ³²	X-ray crystallography
11	286	In SARS-CoV M ^{pro} , Ser284-Thr285-Ile286/Ala mutations enhanced the catalytic machinery by enzyme dynamics	Lim et al., ²²	X-ray crystallography
12	27, 119	Leu27 and Asn119 are involved in the formation of substrate binding site of SARS-CoV M ^{pro}	Xue et al., ¹⁶	X-ray crystallography
13	4	In SARS-CoV M ^{pro} , salt bridge between Arg4-Glu290 stabilizes the dimer	Shi et al., ²⁸	X-ray crystallography
14	126	In SARS-CoV M ^{pro} , Tyr126 is essential for dimer stability and for substrate catalytic machinery via aromatic and hydrophobic interactions between Tyr126 and Met6 and an aromatic interaction between Tyr126 with Phe140	Shi et al., ²⁸	X-ray crystallography
15	126, 141	In SARS-CoV M ^{pro} , 141-140-139 and 126 are directly involved in the dimer formation and regulation, which are required for catalysis	Shi et al., ²⁸	X-ray crystallography, mutagenesis, and ultra-centrifugation
16	141, 185	In IBV M ^{pro} , Gly141 and Asp185 form a substrate binding pocket for the inhibitor N3	Xue et al., ¹⁶ 2008	X-ray crystallography
17	141, 192, 2, 4	Leu141 and Gln192 are in the active site of SARS-CoV M ^{pro} interact with authentic N-terminal residues (Gly2, Arg4, Cys16), enhancing the activity	Xue et al., ²³	X-ray crystallography

18	4, 126	In SARS-CoV M ^{pro} , Arg4Glu mutation produces weak dimer with no activity. Tyr126-M6 hydrophobic interaction stabilizes the dimer conformation	Wei et al., ²¹	Mutagenesis, enzyme assay, and analytical ultracentrifugation
19	286	In SARS-CoV M ^{pro} , Ile286 with other critical dimerization residues form a channel to the catalytic center, which may play a role in regulating catalytic machinery	Shi and Song, ³⁷	Mutagenesis, dynamic light scattering, CD and NMR spectroscopy
20	4, 137	In SARS-CoV M ^{pro} , Arg4 forms dimer interface with Lys137-Gln127 and Glu290	Ghosh et al., ²⁰	X-ray crystallography
21	2, 4	N-terminal (residues 1-4) truncation of SARS-CoV M ^{pro} affects dimer and enzymatic activity	Hsu et al., ¹⁸	Mutagenesis, enzyme assay, and analytical ultracentrifugation
22	2, 4, 126, 286, 295	Gly2, Arg4, Gly126, Glu286, and Gln295 are conserved and play key roles at the dimer interface in the M ^{pro} structures of PEDV, TGEV, and HCoV-229E	Ye et al., ²⁷ ; Anand et al., ²⁵ ; Lee et al., ²⁶	X-ray crystallography, size-exclusion chromatography, and ultracentrifugation

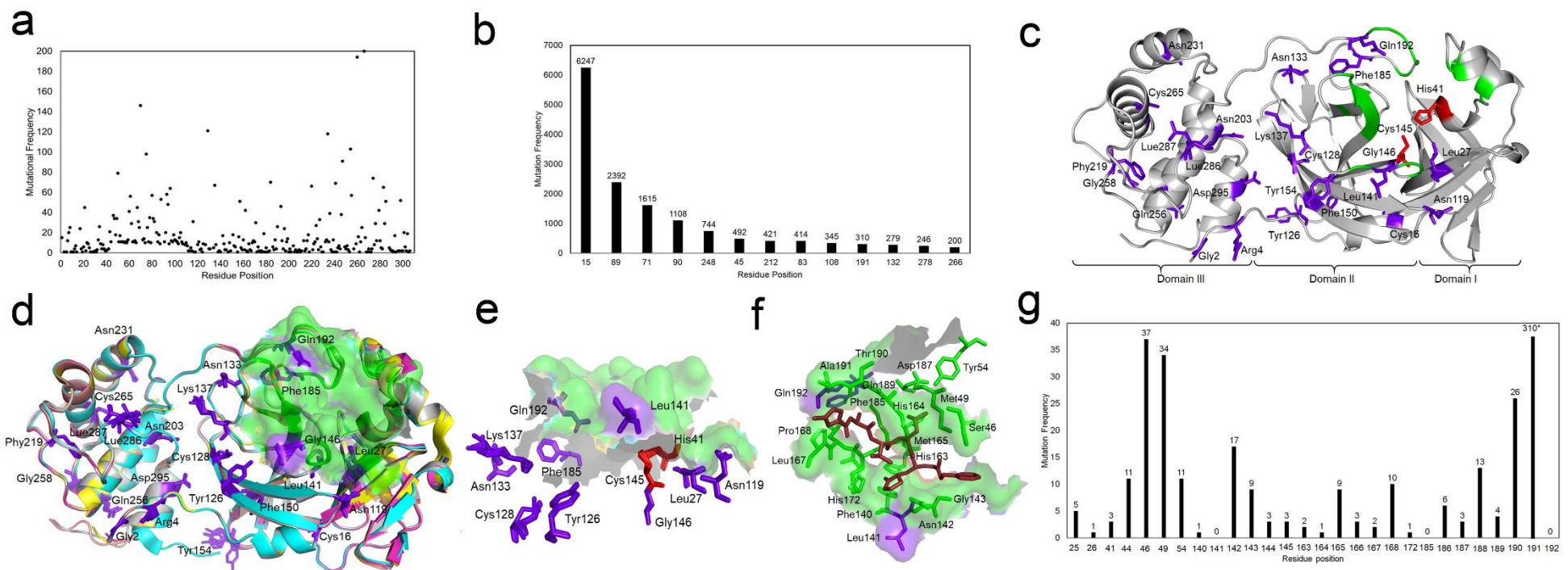
355

356 SARS-CoV: Severe acute respiratory syndrome coronavirus, HKU4: Tylonycteris bat
 357 coronavirus HKU4, PEDV: Porcine epidemic diarrhea virus, HCOV-229E: Human
 358 coronavirus 229E, MERS: Middle East respiratory syndrome-related coronavirus, TGEV:
 359 Transmissible gastroenteritis virus, IBV: Infectious bronchitis virus

360

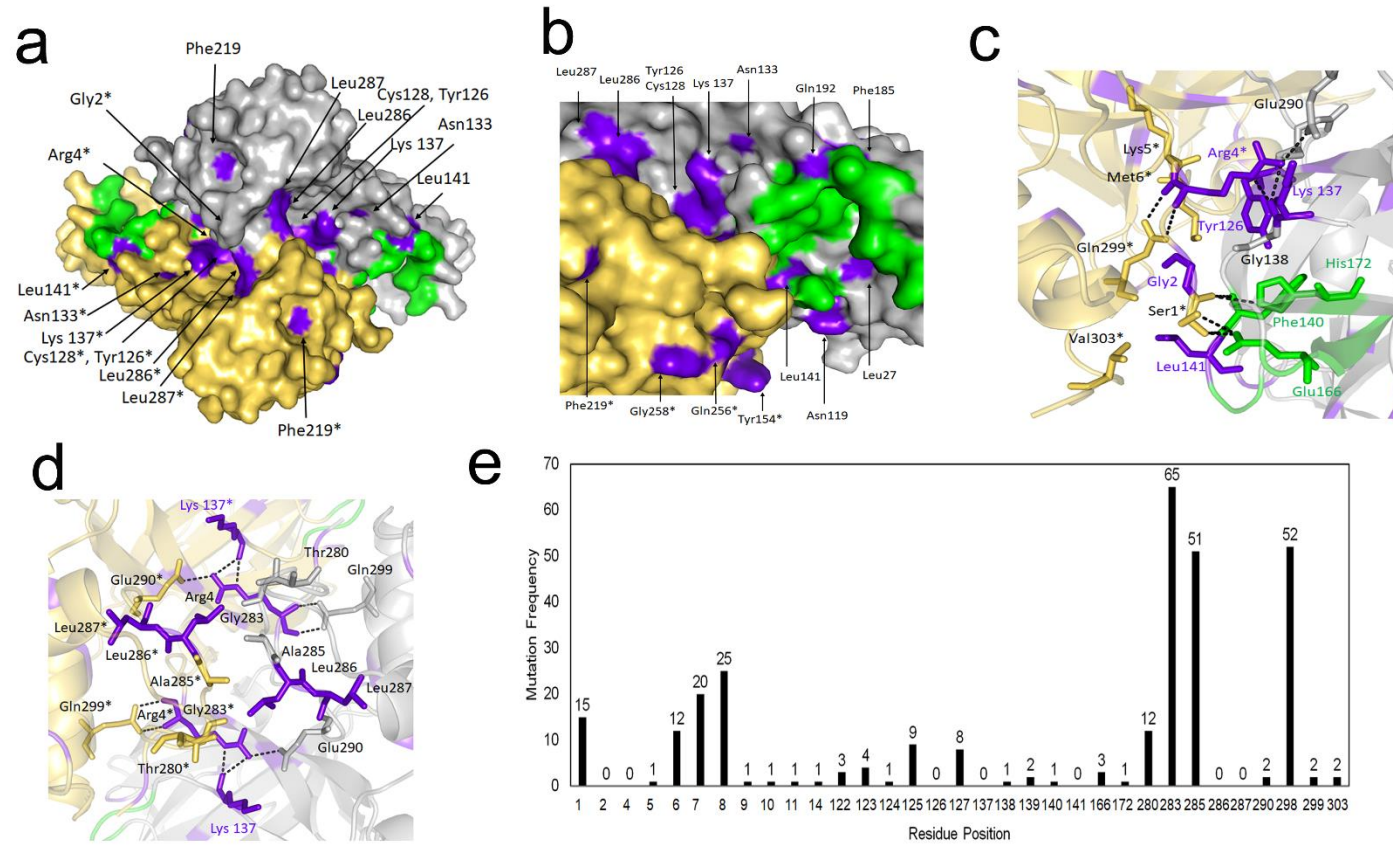
361

362 Figures



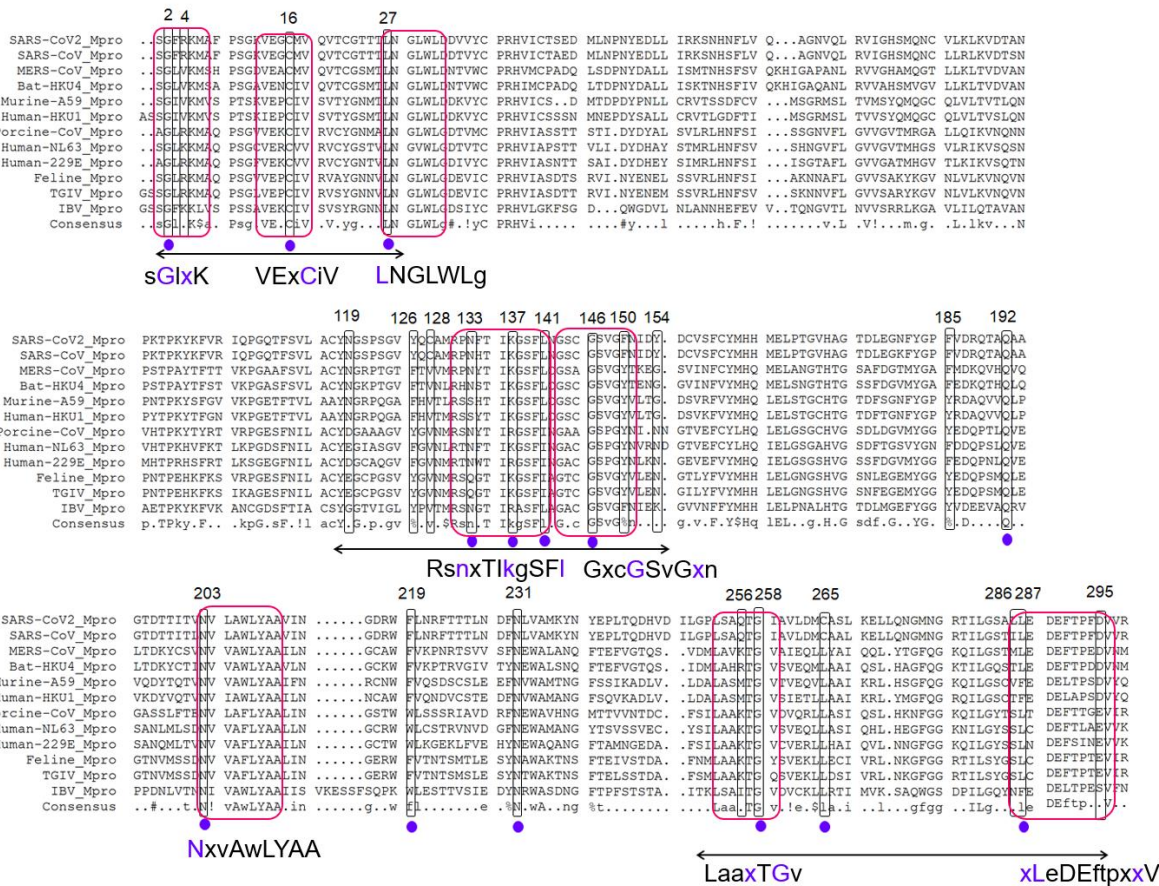
363

364 Figure 1: Hotspots and coldspots in SARS-CoV2 M^{pro}. (a) Residues with less than 200 mutations and (b) residues with more than 200 mutations plotted
365 against mutation frequency. (c) Structural mapping of coldspots (PDB code: 6LU7); (d) Superimposition of high-resolution structures of SARS-CoV2
366 M^{pro}: PDB codes are 6LU7 (grey), 6Y2F (cyan), 6LZE (magenta), 6M0K (yellow), 7BUY (salmon); (e) Coldspots in and around the active sites of the
367 superimposed structures of SARS-CoV2 M^{pro}; (f) Active site pocket in 6LU7 with inhibitor N3 (ruby). (g) Mutational frequency of active site residues.
368 191 Coldspots: purple sticks; active sites: green surface/cartoon; catalytic dyads: red sticks.



369

370 Figure 2: Dimer interface of SARS-CoV2 M^{pro}. (a) Surface model of the dimer (PDB code: 6LU7); (b) Extended and detailed view of panel a showing
 371 the dimer interface, with coldspot residues on the surface model; (c) Site1 and (d) Site2 with coldspot residues and interactions involved in dimerization;
 372 (e) Mutation frequency of dimer interface residues. Grey cartoon/surface: protomer A; Yellow surface/cartoon: protomer B; residues with * are from
 373 protomer B; purple: coldspot residues; green: active site; dashes: hydrogen bonds.



374

375 Figure 3: Multiple sequence alignment of M^{pro} from various coronaviruses. The mutational coldspots of SARS-CoV2 M^{pro} are shown in boxed regions
 376 and red boxed regions are conserved patterns. The purple dots indicate conserved coldspots among all the aligned coronavirus M^{pro}s, and double arrows
 377 indicate the coldspot clusters.